Microchemical Journal 212 (2025) 113471

Contents lists available at ScienceDirect

Microchemical Journal

journal homepage: www.elsevier.com/locate/microc

Experimental evidence of the thermally dominated effect of CW NIR laser irradiation for the restoration of darkened red lead in wall paintings

Amelia Suzuki [a,e,*], Iacopo Osticioli [b], Francesco di Benedetto [c], Werner Oberhauser [d], Haida Liang [e], Francesco d'Acapito [f], Cristiano Riminesi [a]

[a] Institute of Heritage Science, National Research Council, ISPC-CNR, Via Madonna del Piano 10, Sesto Fiorentino (FI) 50019, Italy
[b] Institute of Applied Physics "Nello Carrara", National Research Council IFAC-CNR, Via Madonna del Piano 10, Sesto Fiorentino (FI) 50019, Italy
[c] Department of Physics and Earth Science, University of Ferrara, Via Saragat 1, Ferrara, Italy
[d] Institute of Chemistry of OrganoMetallic Compounds – National Research Council ICCOM-CNR, Via Madonna del Piano 10, Sesto Fiorentino (FI) 50019, Italy
[e] Imaging and Sensing for Archaeology, Art History and Conservation (ISAAC) Lab, School of Science and Technology, Nottingham Trent University, Nottingham NG11 8NS, United Kingdom
[f] CNR-IOM Sez. Grenoble c/o ESRF-LISA CRG 71 Avenue des Martyrs, Grenoble, France

ARTICLE INFO

Keywords:
Pigments
XRPD
XAS
Raman spectroscopy
Lead oxides
Laser treatment
Non-stoichiometric lead oxides

ABSTRACT

In wall paintings, the widely used red lead pigment (Pb_3O_4) may darken due to its transformation to black-brown plattnerite (β-PbO_2). No well-established conversion methods to restore darkened red lead in wall paintings have been reported yet. Only recently, the use of Nd:YAG Continuous Wave (CW) laser irradiation has been proposed and tested on mock-ups and on a wall painting to recover darkened red lead. Although very promising, the method still needs to be fully characterized (penetration depth, stability, by-products etc.). The understanding of the main mechanisms is crucial for the identification of the best operative conditions and to assess the possible risks associated to this method. To identify the laser-induced products and their distribution in the paint layer a combination of synchrotron based (SR) micro X-ray powder diffraction mapping (μ-XRPD), Near-edge X-ray absorption spectroscopy (XANES) at the Pb L_{III} edge, μ-Raman spectroscopy, and VIS-NIR and short wave infrared (SWIR) hyperspectral imaging (400–2000 nm) has been used to characterize the bulk, the surface and the stratigraphy of a plattnerite wall painting mock-up treated with a CW 1064 nm laser. New compounds in the laser-induced treatment of plattnerite have been identified, representing the key evidence of a predominant thermal effect of the laser treatment. These compounds are non-stoichiometric lead oxides that are an intermediate step in the reduction process of plattnerite. A characteristic Raman spectrum of these non-stoichiometric lead oxides was identified with a main band at 419 cm^{-1}. These compounds are found to be surprisingly stable over the 2-year observation period.

1. Introduction

Red lead (Pb_3O_4) is a bright red pigment widely used since antiquity [1]. It is one of the earliest manufactured pigments traditionally produced by calcinating (thermal treatment) for several hours lead white (often a mixture of hydrocerussite $2PbCO_3{\cdot}Pb(OH)_2$ and cerussite $PbCO_3$) [2]. The pigment is a mixed valence state lead oxide with both Pb(IV) in distorted octahedral and Pb(II) at the vertices of irregular pyramids [3]. Owing to the proximity of the temperature at which red lead and lead monoxides (yellow massicot and red–orange litharge, β- and α-PbO, respectively) are produced [4] and the difficulty in the precise control of the effective temperature of the furnaces, lead monoxide impurities are often present in high concentrations, such as 15 % in weight [5]. The presence of these impurities seems to enhance the reactivity of red lead pigment towards discoloration [6,7]. Various types of red lead discoloration have been reported in literature, mainly referred to as darkening and bleaching [2,8]. The identification of the alteration products of red lead and the understanding of the main mechanisms is still an open issue [1,5]. On many wall paintings it has been reported to occur a darkening phenomenon, often ascribed to the transformation of red lead into the beta form of lead dioxide [9–13]. Plattnerite (β-PbO_2) is a brown-black compound particularly studied in electrochemistry for its unusual metallic conductivity primarily due its variable stoichiometry [14] and broadly used for lead acid batteries and

* Corresponding author at: Institute of Heritage Science, National Research Council, ISPC-CNR, Via Madonna del Piano 10, Sesto Fiorentino (FI) 50019, Italy.
E-mail address: mariaameliasuzuki@cnr.it (A. Suzuki).

https://doi.org/10.1016/j.microc.2025.113471
Received 30 January 2025; Received in revised form 21 March 2025; Accepted 24 March 2025
Available online 26 March 2025

as an anode material for electrodeposited coatings [15]. In few cases the α-PbO_2 phase, called scrutinyite (also dark in colour), has also been reported as degradation product in wall paintings [12,16,17]. Owing to the very similar calculated chemical potentials, the presence of one of the two polymorphs seems not distinctive of very different degradation conditions [18].

Several studies were conducted to understand the causes of red lead darkening.[5,6,17,19] The presence of salts (especially $NaHCO_3$) and humidity gave the best artificial ageing results.[17] In acidic solution, red lead was proven to undergo a disproportionation reaction, resulting in the formation of plattnerite and Pb^{2+} in solution [20], which can then form PbO or directly precipitate as a carbonate or sulphate in contact with carbonate or sulphate ions [11]. The darkening is mainly reported as a phenomenon starting from the surface [21], although cases of darkening throughout the stratigraphy or starting from the substrate upwards have been observed [6,22]. In some cases, the red lead darkening is so pronounced that the wall painting totally lose the readability and extensive research has recently focused on virtually reconstruct the original colour scheme [23].

Up to now, no restoration methods to effectively recover the darkened red lead in wall paintings have been established yet and their development are crucial to safeguard the integrity and enhance the readability of artworks. Only in the last two decades, a method based on CW laser irradiation has been tested on mock-ups and in one real wall painting [24,25]. The authors showed that the transformation of plattnerite into red lead occurs at different intensity threshold using 514, 811 and 1064 nm lasers. Undesired formation of lead monoxides was obtained mainly with the 514 nm laser and was ascribed to the higher absorption at this wavelength. Although very promising, the method still needs to be understood and fully characterized. Little is known regarding the treatment penetration depth, the efficacy and level of control of the method, and the stability over time. It has been assumed that the main laser-induced effect is thermal but has not yet been correlated to experimental evidence. The understanding of the main mechanism is very important to improve the laser operative conditions and to better evaluate the risks associated with such restoration treatment. To gain suitable experimental information concerning the laser induced PbO_2 to Pb_3O_4 conversion, an in-depth characterization of a plattnerite wall painting mock-up irradiated with a 1064 nm CW was carried out with a multi-analytical approach, using VIS-NIR and SWIR hyperspectral imaging, μ-Raman, SR based μ-XRPD and X-ray absorption spectroscopy.

2. Experimental section

2.1. Mock-ups and experimental design

A wall painting mock-up was made applying a chemical grade plattnerite powder (ACROS 97 % purity grade) in animal glue on a lime mortar substrate. Samples of the same plattnerite powder were used to perform the heat treatments to compare the products with the ones obtained by laser treatment. For the laser irradiation tests, a Nd:YAG CW 1064 nm Spectrum Stabilized Single-Mode laser with output power ~ 300 mW was used with a spot size (FWHM) of 450 and 200 μm. The surface temperature of the tests performed with the 450 μm laser spot was monitored with the thermally controlled Raman system (for details [26]) allowing to monitor the average surface temperature from an area ~ 1.5 bigger than the spot size during the irradiation.[27] At first, tests varying the laser power and spot size were carried out to identify the suitable condition for an effective transformation. When a visible effect was observed under the microscope, μ-Raman spectroscopy, VIS-NIR and SWIR hyperspectral imaging were performed on the surface of the sample fragments. Once determined the best intensity (254 W/cm^2) with a 200 μm spot size (FWHM), a treatment area of 10 × 3 mm^2 was made by continuous scan irradiation in consecutive lines and extensively analysed both from the surface and on thin sections of the stratigraphy with the techniques described below.

2.2. Variable temperature XRPD

The chemical grade plattnerite powder samples were heated up in an Anton Parr cell mounted on a diffractometer applying either a nitrogen or air atmosphere. The heating rate used were 20 °C/min and 150 °C/min with a cooling rate of −50 °C/min. The diffractograms were collected at room temperature, then every 20/50 °C above 350 °C, and then remeasured after cooling down. The black solid product formed with the fast-heating rate up to 410 °C was re-measured over 2 years for stability check. The diffraction patterns were collected after each temperature step increase in a Bragg-Brentano geometry with a Cu anode PanAlytical X'Pert Pro diffractometer (40 mA and 40 kV), at a scan speed of 0.14°/s and step size of 0.013°.

2.3. μ-Raman spectroscopy

An XPlora Horiba μ-Raman instrument was used with a 785 nm laser, with a diffraction grating of 1200 l/mm (spectral resolution of 4 cm^{-1}) and a 100 × objective. The laser spot size at the focal point was around 1.5 μm and the power on the sample around 0.4 mW. Raman spectra were acquired using 300 s acquisition time. Wavelength calibration was performed on a standard silicon wafer.

2.4. VIS-NIR and SWIR hyperspectral imaging

Each laser treated area of the plattnerite mock-up was scanned with a SWIR and a VIS-NIR grating-based hyperspectral imaging systems (HSI), the latter developed by ISAAC lab [28]. The line-scan SWIR imaging system is a NEOHySpex SWIR-384 hyperspectral camera with a 16-bit cooled HgCdTe(MCT) sensor. operating in the range 930–2500 nm with a spectral resolution of 5.45 nm. The spatial resolution is ca. 70 μm at a working distance of 10 cm in a microscopic setup. The VIS-NIR (400–1000 nm) HSI consist of an Andor Zyla 5.2 sCMOS camera combined with a Specim ImSpector V10E spectrograph, coupled with a telescope, simultaneously measuring 1000 reflectance spectra along a line of 1500 × 15 $μm^2$ on the target at a distance of 3 m. As illumination source, a tungsten DC light was placed at 45° and at 60 cm. All data were calibrated over a Spectralon© 99 % diffuse reflectance white standard.

2.5. SR high lateral resolution μ-XRPD

To assess the changes in the crystal structure of the laser treated area, SR μ-XRPD mapping was performed at the μ-brunch of ID13 at the European Synchrotron Facility (ESRF, Grenoble, Heritage Historical Materials BAG access [29,30]. Petrographic thin sections were prepared with a support in polycarbonate obtaining thickness of ca. 50 μm. Raster scanning maps were performed with a beam size of ca. 2.5 × 2.5 $μm^2$, a step size of 2 μm in both horizontal and vertical directions, an acquisition time per point of 10 ms at 12.92 keV (0.95967 Å) and a flux of ~ 1.9 × 10^{11} ph/s (at I = 34 mA electron beam current). The two-dimensional diffraction patterns collected in transmission were azimuthally integrated using dedicated Jupyter notebooks, based on the PyFAI software package [31] and were then analysed with PyMCA software to perform ROI imaging [32]. This way, RGB false colour correlation maps are generated based on the intensity of a diagnostic diffraction peak of a specific phase, defining a ROI in the 2θ range. Average diffraction patterns were then extracted from the heat map generated by a single 2θ ROI or from specific portions of the stratigraphy. The identification of the crystalline compounds was then performed with Match! software using COD inorganics database.

2.6. X-ray absorption spectroscopy

XAS with detail in the near structure (XANES) was performed at the

L_{III}–edge of Pb (13035 eV). The measurements were first performed at the Italian BM08-LISA beamline [33] at ESRF to simultaneous acquire the Total Electron Yield (TEY), fluorescence yield and, when possible, the transmission signal. The shorter electron escape depth (tens of nm) of TEY compared to fluorescence mode, gives information from the very top surface of the irradiation volume [34], providing indirect indication of the depth Pb speciation of the laser-transformed volume. XANES were acquired with a beam spot of ~70 × 100 μm^2 with a flux of ~10^9 ph/s with a Si(3 1 1) crystal monochromator. Simultaneous measurement of metallic lead placed after the sample was performed for energy calibration (position of the first inflection point taken at 13035 eV). The wall painting mock-ups were mounted on a specific TEY sample holder [35] with carbon tape and measured rotated 20° with respect to the incoming beam. A collecting anode polarized at ~20 V was placed at about 10 mm from the sample and the chamber was filled with He (0.5 atm). All the acquisitions were repeated 3 times on each spot and data processing was performed with ATHENA [36] to merge, normalize and background subtract each set of XANES.

High energy resolution XANES spectra in fluorescence mode were then acquired at the French BM16-FAME-UHD beamline at ESRF with a multi bunch beam of 200 × 100 μm^2 (horizontal × vertical) with a flux of ca. 10^{11} ph/s in ambient condition using a Si(220) double crystal monochromator (energy calibration performed on a Pb foil in transmission). The samples were positioned 45° with respect to incident beam. The higher energy resolution (1 eV) allowed to differentiate the spectral features of the lead oxides enabling a reliable semi-quantitative analysis of the compounds present over an area of 200 × 1500 μm^2. Deconvolution of the XANES spectra was carried out by linear combination-least squares fitting (LCF) of the standard lead compounds. The pellet standards (15 % wt in cellulose) were measured in fluorescence mode. The standards of red lead (Pb_3O_4) and plattnerite (β-PbO_2) are chemical grades, whereas litharge (α-PbO) and massicot (β-PbO) were synthesized based on the procedure in [37]. All the standards were pre-characterized with XRPD for purity check. The total amount of associated phases resulted below ~ 5 wt%, corresponding to the conventionally assumed detection limit of secondary phases in XANES analysis [38]. The LCF of the experimental processed XANES spectra using the adopted set of standard spectra was performed with the IFEFFIT module in ATHENA[36]. The number of reference spectra to be included in the final LCF (set to 4) was chosen as the minimum number able to introduce a significant reduction of the overall χ^2 value (i.e. change by more than 20 %).

3. Results and discussion

3.1. Characterization of the thermal treatment

Two variable temperature XRPD (VT-XRPD) experiments at a heating rate of 20 °C/min were carried up to 500 °C (Fig. 1) and up to 600 °C (Table 1), showing consistent results regarding the crystallization of several lead oxides. Between room temperature and 350 °C the diffraction pattern of plattnerite remained unchanged. At 370 °C, new double peaks start to form, becoming very intense at 410 °C, when almost all the plattnerite diffraction peaks disappeared. These double peaks can be ascribed to non-stoichiometric lead oxides [39–41], that are intermediated states in the thermal transformation of plattnerite into red lead and that from now on will be called Pb_xO_y. At 410 °C, small diffraction peaks ascribed to red lead appeared and the quasi-complete transformation to red lead is obtained at 500 °C. Above 500 °C, both polymorphs of PbO are formed. After cooling no further changes in phase composition were detected (Table 1). These experiments were carried out in nitrogen environment; repeating the experiments in air showed no changes, suggesting that oxygen do not play a role in the lead oxides thermal transformation.

A fast thermal experiment was also conducted at a heating rate of 150 °C/min up to 410 °C. The powder produced by this fast heating appears black in colour and is mainly composed of the intermediate non-stoichiometric lead oxides (Pb_xO_y). By observing the powder under high magnification, at least 2 optically distinctive particles are visible, bright red and black-grey particles (Fig. 1b). The μ-Raman spectra collected from these two distinctive coloured particles show specific spectral features (Fig. 1c): on the red grains all the characteristic peaks of red lead are present but all red-shifted; on the black grains the spectrum is characterized by a main broad band at 418 cm^{-1} and a weak band at 122 cm^{-1}. The red shift of the frequencies of the red grains, that varies between 6 and 10 cm^{-1} compared to red lead, could indicate an increase

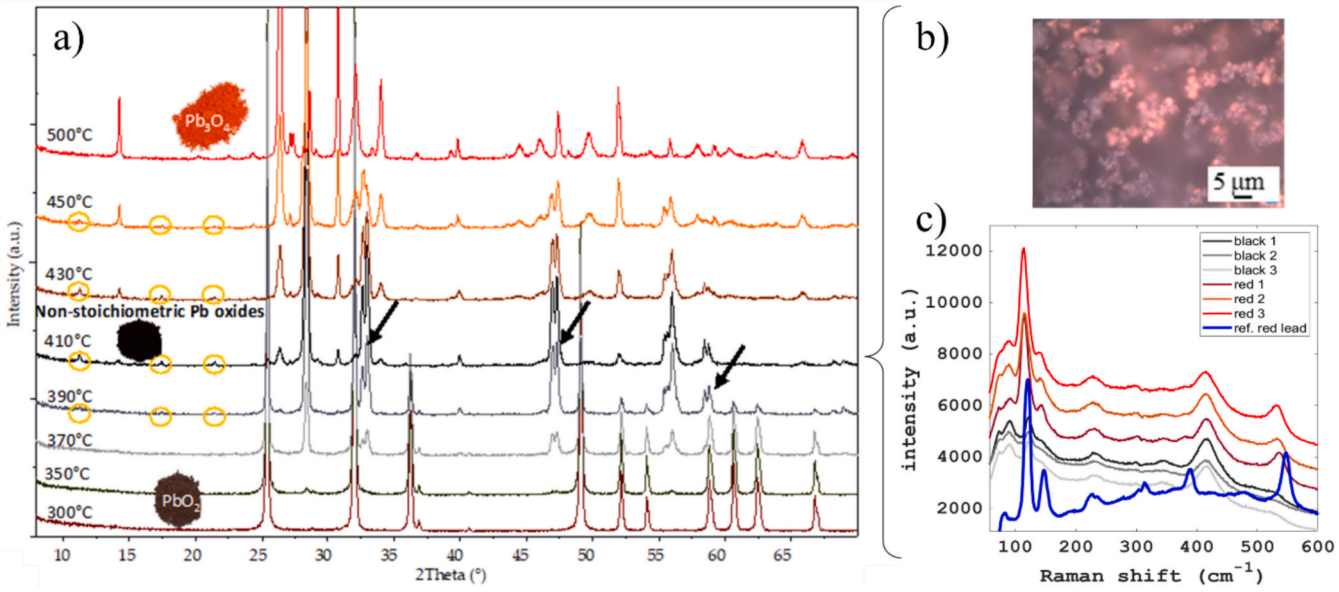

Fig. 1. a) VT-XRPD of plattnerite powder heated up to 500 °C at 20 °C/min in nitrogen atmosphere. The black arrows and the yellow circles indicate the double peaks and the law intensity peaks, respectively appearing during the transformation of β-PbO_2 to Pb_3O_4. b) Microscope image of the black powder of non-stoichiometric lead oxides obtained by fast heating of plattnerite up to 410 °C at 150 °C/min. In c) the μ-Raman spectra collected on some red (red lines) and black grains (black and grey lines) of image b). In blue a reference spectrum of red lead. (For interpretation of the references to colour in this figure legend, the reader is referred to the web version of this article.)

Table 1
Summary of the lead phases identified during a VT-XRPD experiment on plattnerite powder up to 600 °C in nitrogen atmosphere at 20 °C/min.

Temperature (C°)	25–350	370–390	410–450	500	550	600	25 *
Phases identified with XRPD	β-PbO_2	Pb_xO_y, β-PbO_2	Pb_xO_y, Pb_3O_4	Pb_3O_4	Pb_3O_4, α-PbO, β-PbO	β-PbO	β-PbO

* at the end of cooling.

of the bond length of the structure.

3.2. The laser-induced transformation of plattnerite into red lead

The first visual effect when irradiating with the 1064 nm laser the plattnerite wall painting mock-up was noticed when applying an intensity of 220 W/cm^2 with a spot size of 450 μm for 1 min (Fig. 2). A temperature plateau was reached after few seconds and no further visible changes appeared on the sample after prolonged exposure. This suggests that the duration of the irradiation is a negligible parameter. The average surface temperature measured over a region of 1.5 times the laser spot area is 330 °C. Thus, the temperature at the centre of the irradiated area is most likely to have reached a temperature greater than the one required to start the transformation of plattnerite (370 °C, based on Table 1). The irradiated area appears darkened with few red grains at the centre of the spot (Fig. 2a). Multiple μ-Raman spectra acquired on the darkened area reveal a consistent spectrum characterized by a main band at 424 cm^{-1} and weak bands at 129 cm^{-1}, 239 cm^{-1} and 355 cm^{-1}, while on the red grains the spectra show the main characteristic peaks of red lead in addition to the peaks found on the black area (Fig. 2b). In the VIS-NIR spectra, the plattnerite surface is characterized by a specific increase of reflectance around 750–800 nm (Fig. 2c), that has been reported from wall paintings containing plattnerite [42] and synthetic reference powders [9,25] only very recently. This feature at 750–800 nm gradually shifts towards longer wavelength and increases in reflectance towards the centre of the spot. In the SWIR spectra, an absorption band at around 1280 nm and one at 1800 nm characterize the plattnerite surface (Fig. 2d). The former absorption band gradually disappears towards the centre of the irradiated spot (Fig. 2d). The first literature reporting an absorption spectrum in the range 400–2500 nm of lead dioxides disclose a strong absorption band at 1290.32 nm (0.94 eV) for plattnerite [43]. In cultural heritage field, this SWIR absorption band has never been detected, either because often the probed spectral range did not reach the SWIR spectral region [9,25], or even if recorded, as in the case of [42], the signal might have been masked by the contribution of some other compounds in the wall painting. Indeed, we observed that the presence of small amount of red lead formed on the surface of plattnerite can mask this feature (Fig. 2).

To reach higher laser intensity values, multiple irradiation tests were carried out by performing line scans using a 200 μm spot size and varying the laser power (Fig. 3a-d). From 254 W/cm^2 a very homogeneous red layer was produced upon irradiation (Fig. 3b) and the μ-Raman spectra confirmed the presence of red lead (Fig. S1a). By further increasing the laser intensity, the shift from black to red is also

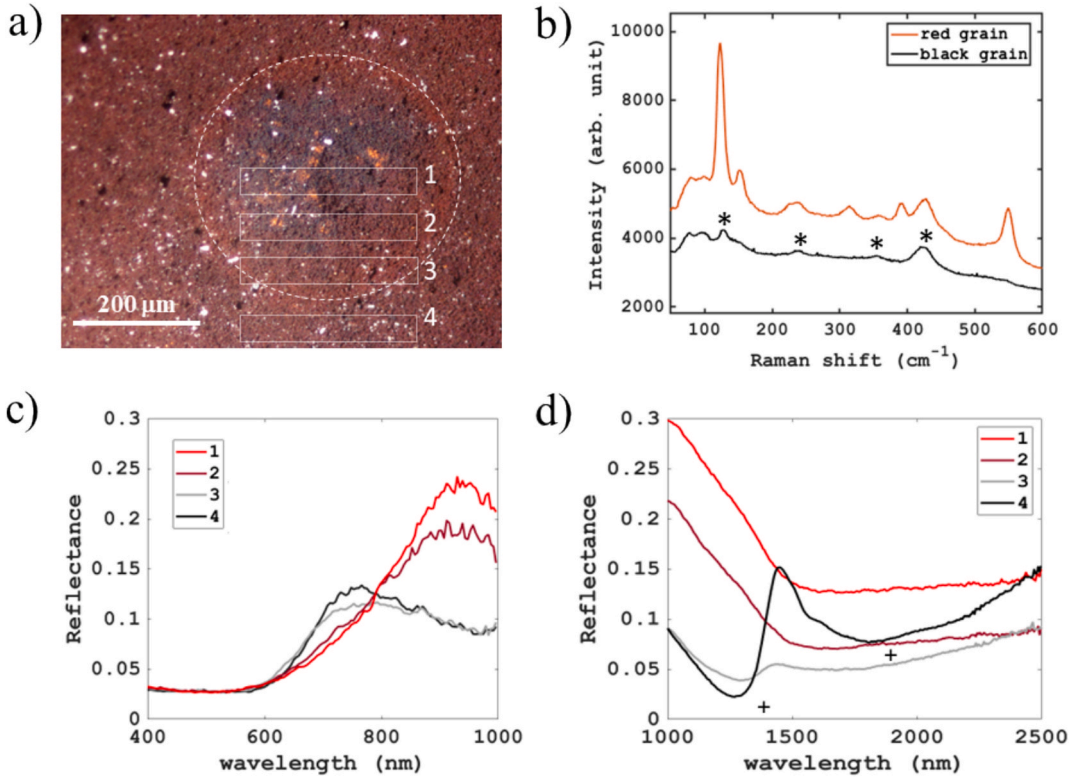

Fig. 2. a) The stereomicroscope image of the plattnerite mock-up irradiated on a single spot with a 1064 nm CW laser for 5 s with a spot size of 450 μm and an intensity of 220 W/cm^2. b) The Raman spectra collected on a black and a red grain in the irradiated area with * indicating the new bands identified in the black grains. c) The VIS-NIR and d) the SWIR reflectance spectra, extracted from different areas of the irradiated spot as indicated in figure a) (1,2,3 inside the laser spot and 4 outside the laser spot on the pristine plattnerite). SWIR absorptions bands identified on the plattnerite paint surface are marked with '+'. (For interpretation of the references to colour in this figure legend, the reader is referred to the web version of this article.)

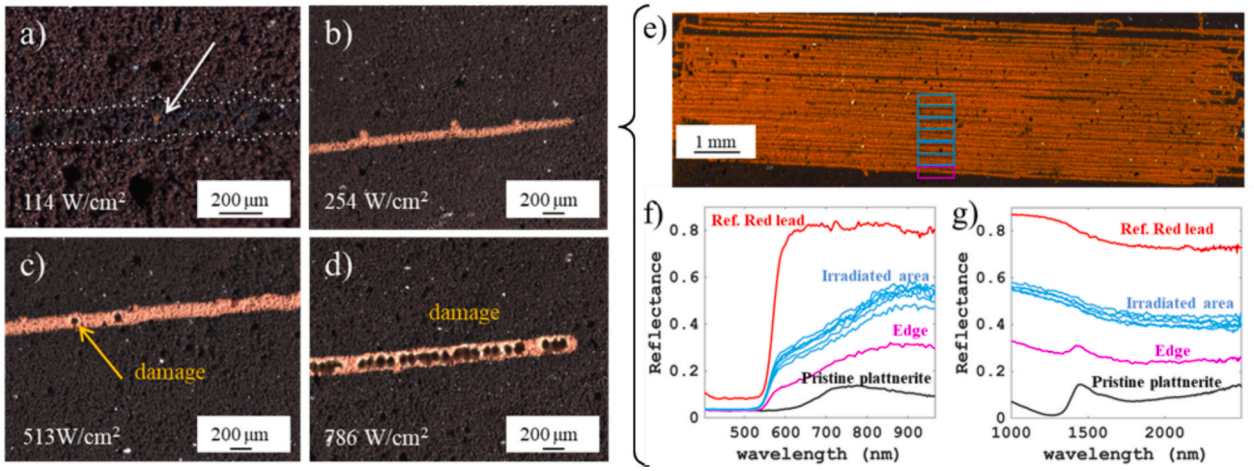

Fig. 3. a–d) the line scan irradiation tests on the plattnerite in animal glue wall painting mock-up with the 1064 nm CW laser with a spot of 200 µm and a maximum duration per point of 5 s, at increasing intensity. e) The stereo microscope image of the wide irradiated area using the optimum intensity of 254 W/cm^2. f) The VIS-NIR reflectance spectra extracted from the pristine plattnerite mock-up (in black), from the edge between treated and untreated area (magenta) and from various consecutive areas within the treated area (light blue curves). A reference spectrum of red lead is also shown for comparison (red curve). g) The same areas measured with the SWIR hyperspectral imaging system. (For interpretation of the references to colour in this figure legend, the reader is referred to the web version of this article.)

followed by the formation of sporadic craters (Fig. 3c). With even higher laser intensity this type of damage became widespread (Fig. 3d), with the edges of the craters composed of yellow particles of massicot (Fig. S1b), indicating an excessive reduction.

Even by prolonging the exposure up to 30 s with 254 W/cm^2 and a spot size of 200 µm, only red particles appear on the surface, therefore this operative condition was considered optimum to carry out further characterization of the laser treatment. In a recent work 15 W/cm^2 was identified as effective intensity for the treatment of a pressed plattnerite powder pellet using a 1080 nm diode laser [25]. This intensity is a factor 16 smaller compared to the one identified in the present work, but it is important to consider that in Seauve et al. [25] the experiment was conducted using 2.9 mm (FWHM) spot size compared to 200 µm spot size in our current experiment. In a recent work [44] during the irradiation of a vermilion oil mock-up the temperature rise was found to reach 40 °C when using a spot size of 200 µm, and up to 140 °C when using a spot of 1 mm under the same intensity using a 785 nm laser. This shows how the effective intensity range can significantly change due to the laser spot size. In the same work [44] it was also found that the presence of a binder changes the temperature rise compared to the irradiation of a pigment only. Therefore, the specific material composition [44,45], as well as the particle size of the pigment [46,47], and the optical properties of the material (e.g. roughness) can also affect the optimum intensity. Thus, the intensity range found in our experiment is an indication only.

In Fig. 3e is reported the wide scan treatment area of 10 × 3 mm^2 obtained with the optimum irradiation condition. The HSI analysis of the red area reveals the shift towards longer wavelength of the characteristic feature of plattnerite at around 750–800 nm (Fig. 3f). At the same time a clear point of inflection of red lead appears at around 550 nm (Fig. 3f). In the SWIR spectral range, the absorption band of the pristine plattnerite surface around 1280 nm disappears in the irradiated area containing red lead (Fig. 3g).

The simultaneous acquisition of TEY and fluorescence mode XANES at the Pb L_{III} edge on single points of the wide-treated area reveals a consistent change of the TEY spectra compared to the fluorescence signal (Fig. 4a), demonstrating the stratification nature of the irradiated volume. The probed depth of the TEY has been estimated to be ca. 120 nm while the fluorescence signal results from ca. 15 µm (SI for calculation details). High energy resolution XANES spectra on 10 consecutive spots over a line of 1.5 mm reveal a consistent spectrum compared to the pristine plattnerite (Fig. 4b), indicating a homogeneous laser treatment. The fluorescence signal in this case is obtained at 45°, corresponding to a probed depth of ca. 30 µm. The linear combination fit with the standard lead phases (Fig. 4c) of these spectra reveals that within the probed volume a constant 40 % is composed of PbO_2, followed by a ~ 30 % of Pb_3O_4, ~15 % of PbO and a few percent of metallic Pb (Fig. 4d) with an average Pb redox state of + 3 (Fig. S2).

The XANES results agree with the SR µ-XRPD mapping carried out on a thin section obtained from the irradiated area (Fig. 5a). The first optically red 15–20 µm of the overall 200 µm plattnerite paint layer of the mock-up is composed of red lead, with some traces of massicot (β-PbO). An intermediate layer of ca. 15 µm between the surface layer of red lead and the unreacted bulk of plattnerite is characterized by the presence of the same double peaks as the one identified in the VT-XRPD experiment (Fig. 1) and ascribed to non-stoichiometric lead oxides (Pb_xO_y), co-present with main diffraction peaks of plattnerite and red lead (Fig. 5b, d). The same thin section was measured by µ-XRPD after 2 years since the laser treatment and the distribution of the crystalline compound did not change.[30] The µ-Raman spectra acquired on this intermediate Pb_xO_y layer reveal a distinctive strong broad band at 419 cm^{-1}, a medium band at 122 cm^{-1} and weak bands at 228 cm^{-1}, 352 cm^{-1} and 540 cm^{-1} (Fig. 5c). The same bands were detected in the Pb_xO_y powder obtained with the fast thermal treatment of plattnerite (Fig. 1c). In the literature, a similar main band at 410 cm^{-1} was detected during the laser-induced transformation of plattnerite irradiated with multiple laser wavelengths [48,49]. While a 426 cm^{-1} band was detected after [50] and during [48] a thermal treatment up to 400–450 °C, and the compound has been attributed by means of XRPD to $PbO_{1.55}$ and $PbO_{1.57}$, respectively. Thus, the peak position is not necessarily comparable and the XRPD attribution is unclear. One of the possible known intermediate lead oxides is the lead sesquioxide, Pb_2O_3 [51]. The Raman spectra of several sesquioxides for the lanthanide elements is characterized by the main band between 380 and 400 cm^{-1} and for higher f electrons and higher atomic number, like in the case of lead, the band shift to higher wavenumbers. It would therefore seem reasonable to assign the experimental band at 419 cm^{-1} to Pb_2O_3. However, the latter has a clear different crystalline structure [40] not matching the XRPD patterns and is bright orange in colour, while the Pb_xO_y are clearly black in colour. Although the present experimental evidence does not allow a definitive assignment, the band at 419 cm^{-1} clearly represents a marker for Pb_xO_y formed during the reduction of

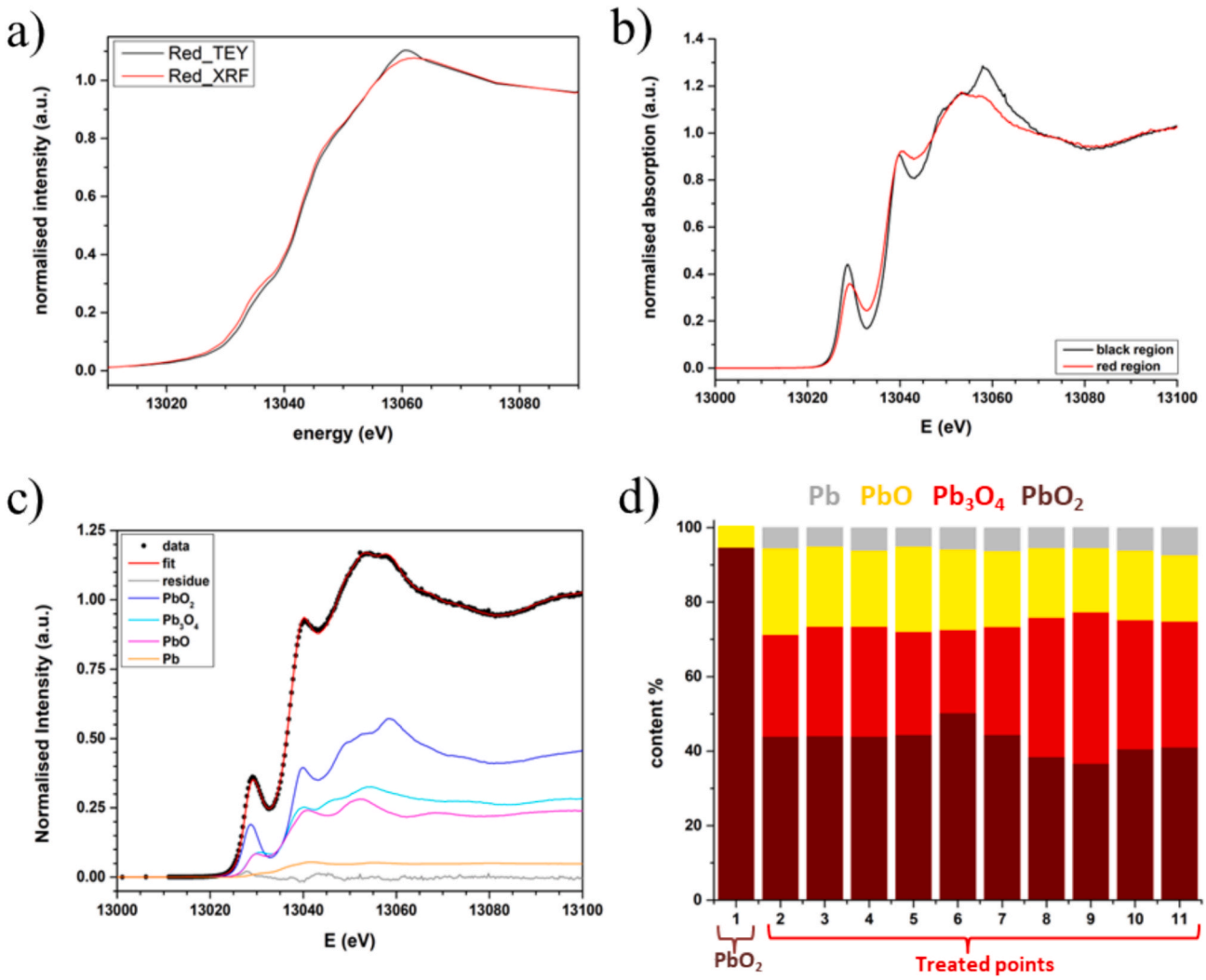

Fig. 4. a) Comparison of TEY and fluorescence spectra, with detail on the edge, simultaneously acquired at BM08 on the red area of the laser treated plattnerite mock-up of Fig. 3e. b) Comparison of high energy resolution XANES acquired at BM16 on the laser treated (red region) and non-irradiated portion (black region) of the same mock-up. c) Example of a LCF with the relevant standards of a XANES spectrum of the red region. d) The lead compounds content % based on the LCF obtained on the non-irradiated portion of the mock-up (spectrum 1) and on 10 consecutive points on the laser treated area (spectra 2–11). (For interpretation of the references to colour in this figure legend, the reader is referred to the web version of this article.)

plattnerite into red lead. Therefore, Raman spectroscopy could be used to monitor the formation of the precursor of red lead, helping in the identification of the suitable operative conditions for a laser treatment *in situ*.

4. Conclusions

This work aimed at shedding light on the efficiency and mechanism behind the recently proposed method to restore darkened red lead wall paintings via CW laser irradiation to convert plattnerite into red lead. The combination of SR μ-XRPD mapping, XANES and μ-Raman spectroscopy allowed a clear characterization of the laser-induced products. New compounds in the laser-induced treatment of plattnerite have been identified, representing the key experimental evidence of the predominant thermal effect of the CW 1064 nm laser treatment of plattnerite. Apart from red lead, in a sub-surface reaction layer, non-stoichiometric lead oxides were identified, showing an un-expected long term (up to 2 years) stability; and their formation could be of interest in other applications beyond the cultural heritage field. The temperature required for an effective transformation is between 400 and 500 °C. Therefore, a highly controlled laser treatment is required for an efficient conversion. Future work will aim at investigating the safety of such temperature range for the surrounding materials present in darkened red lead paint layer. For instance, when red lead is applied in common mixture with lead white or vermilion, these pigments may alter due to their low decomposition temperature (ca. 250 °C [52] and ca. 360 °C [53] respectively); but when mixed with red ochre, its higher thermal stability [54] may result in a safer treatment. In any case, it is worth noting that a laser spot size of just 200 μm led to a very thin red lead layer (20 μm) demonstrating that the conversion is confined, and it could be reasonably controlled. Moreover, the smaller the beam, the easier it is to intervene locally in small, localized portions of the painting affected by darkened particles, especially in cases of very diluted pigment. To better identify the safest efficient laser operative condition while minimizing the risks *in situ*, two monitoring techniques have been identified. A macro-scale VIS-SWIR hyperspectral imaging investigation is suitable to identify and localize the presence of plattnerite. While Raman spectroscopy enables a micro-scale identification of the precursors of red lead, thanks to the characteristic band at 419 cm^{-1} of the non-stoichiometric lead oxides.

Overall, this work contributes to a better understanding of the laser-pigment interaction and represents a valuable base to open the

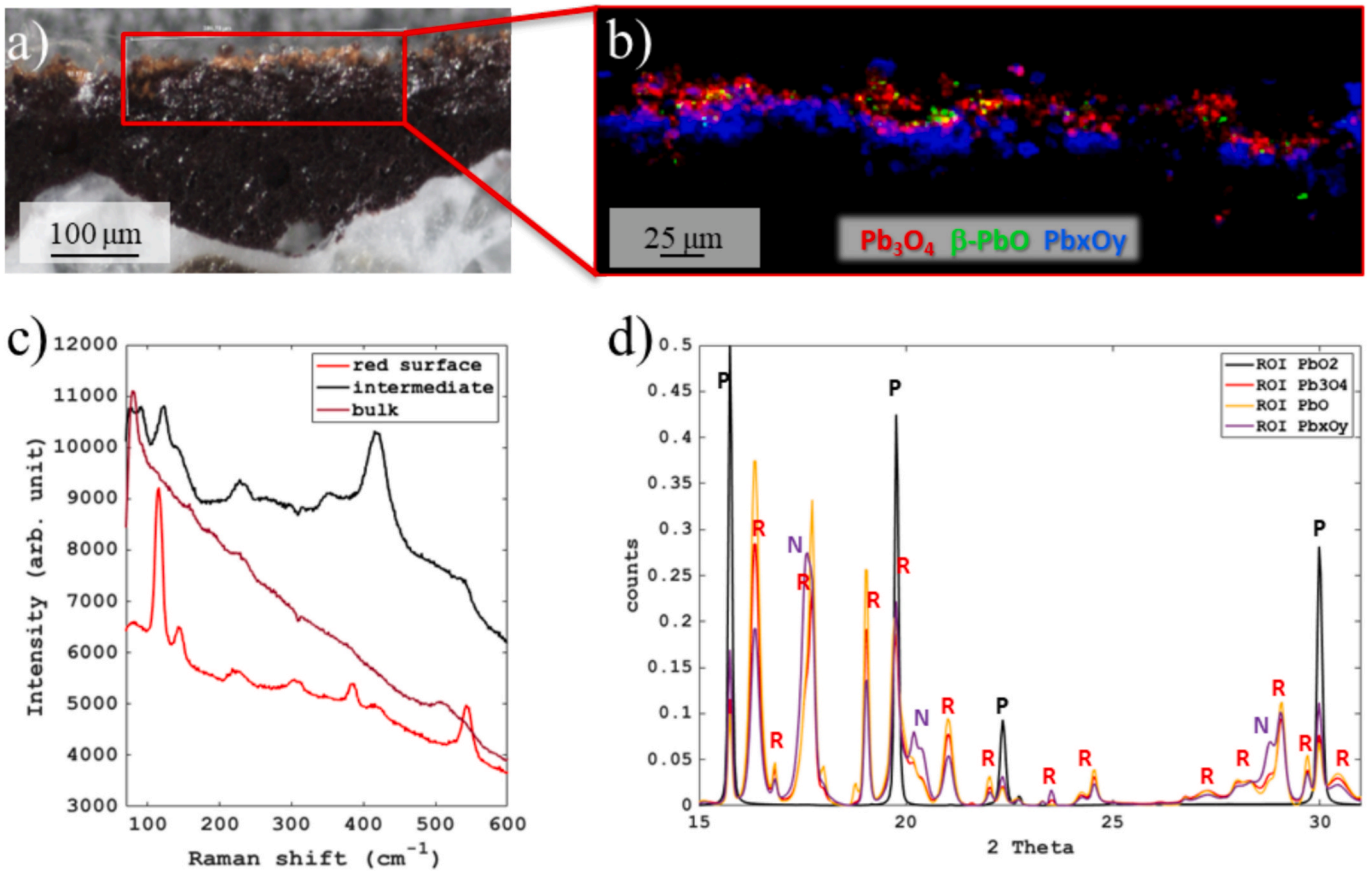

Fig. 5. a) The stratigraphic thin section of the laser treated plattnerite mock-up. b) The ROI imaging RGB combination map of red lead (**R** Pb_3O_4, d = 3.379 Å), massicot (**G** β-PbO, d = 2.945 Å), and intermediate lead oxides (**B** Pb_xO_y d = 2.717–2.737 Å). c) Raman spectra from the surface (red line, corresponding to Pb_3O_4), from the intermediate layer (black line, corresponding to Pb_xO_y), and from the bulk (brown line, corresponding to the weak signal of plattnerite). d) The average patterns obtained from ROI imaging of the different phases. The main peaks of β-PbO_2 (**P**), Pb_3O_4 (**R**) and Pb_xO_y (**N**) are reported. (For interpretation of the references to colour in this figure legend, the reader is referred to the web version of this article.)

discussion with conservators and the heritage science community regarding the suitability of such restoration interventions in real wall paintings.

5. Funding resources

This work was supported by the IPERION HS project funded by European Union's Horizon 2020 research and innovation programme under GA n. 871034; the UK Arts and Humanities Research Council (AHRC AH/V012460/1); and the Tuscany Region (POR FSE 2014-2020) in the framework of PLas@rt project Innovative techniques for the conservation based on laser ablation and non-thermal plasma method. AS acknowledge Nottingham Trent University for her PhD studentship funding.

CRediT authorship contribution statement

Amelia Suzuki: Writing – review & editing, Writing – original draft, Visualization, Validation, Methodology, Investigation, Formal analysis, Data curation, Conceptualization. **Iacopo Osticioli:** Writing – review & editing, Methodology, Investigation. **Francesco di Benedetto:** Writing – review & editing, Visualization, Validation, Investigation, Formal analysis. **Werner Oberhauser:** Writing – review & editing, Investigation. **Haida Liang:** Writing – review & editing, Supervision, Methodology, Funding acquisition. **Francesco d'Acapito:** Writing – review & editing, Visualization, Validation, Investigation, Formal analysis. **Cristiano Riminesi:** Writing – review & editing, Supervision, Methodology, Funding acquisition, Conceptualization.

Declaration of competing interest

The authors declare that they have no known competing financial interests or personal relationships that could have appeared to influence the work reported in this paper.

Acknowledgements

This publication is dedicated to the memory of Vincent Detalle who pioneered the study of the conversion of plattnerite back to red lead using laser tratment. We acknowledge the European Synchrotron Radiation Facility for provision of synchrotron radiation facilities (proposals HG-191, HG-175, BAG "Historical materials" HG-172 and HG-213) and we would like to thank Mauro Rovezzi for his help during BM16 measurements, Manfred Burghammer and Jiliang Liu for assistance in using ID13. Salvatore Siano is gratefully acknowledged for the provision of the CW laser system for the laser treatment experiments. We also thank Florence Liggins for the help during the collection of the SWIR imaging data and Andrea Marchionni for his help during the synthesis of the lead monoxides standards.

Appendix A. Supplementary data

Supplementary data to this article can be found online at https://doi.org/10.1016/j.microc.2025.113471.

Data availability

All data are available in the main text or the supporting information. Raw data can be made available upon reasonable request. The raw μ-XRPD data are available in the ESRF repository DOI10.15151/ESRF-DC-2115831341.

References

[1] E. Gliozzo, C. Ionescu, Pigments—Lead-based whites, reds, yellows and oranges and their alteration phases, Archaeol. Anthropol. Sci. 14 (2022), https://doi.org/10.1007/s12520-021-01407-z.

[2] E. West Fitzhugh, Red lead and Minium, in: R.L. Feller (Ed.), Artists' Pigments : A Handbook of Their History and Characteristics, Archetype Publications, Washington, 1986: pp. 109–140.

[3] A. Amat, F. Rosi, C. Miliani, P. Sassi, M. Paolantoni, S. Fantacci, A combined theoretical and experimental investigation of the electronic and vibrational properties of red lead pigment, J. Cult Herit. 46 (2020) 374–381, https://doi.org/10.1016/j.culher.2020.04.014.

[4] K. Gavrichev, A. Bolshakov, D. Kondakov, A. Khoroshilov, S. Denisov, Thermal transformations of lead oxides, J. Therm. Anal. Calorim. 92 (2008) 857–863, https://doi.org/10.1007/s10973-007-8590-x.

[5] S. Aze, J.M. Vallet, V. Detalle, O. Grauby, A. Baronnet, Chromatic alterations of red lead pigments in artworks: A review, Phase Transit. 81 (2008) 145–154, https://doi.org/10.1080/01411590701514326.

[6] S.V. Aze, A. Baronnet, O. Grauby, Red lead darkening in wall paintings: natural ageing of experimental wall paintings versus artificial ageing tests, Eur. J. Mineral. 19 (2007) 883–890, https://doi.org/10.1127/0935-1221/2007/0019-1771.

[7] E. Ayalew, K. Janssens, K. De Wael, Unraveling the Reactivity of Minium toward Bicarbonate and the Role of Lead Oxides Therein, Anal. Chem. 88 (2016) 1564–1569, https://doi.org/10.1021/acs.analchem.5b02503.

[8] D. Saunders, J. Kirby, The effect of relative humidity on artists' pigments, Natl. Gallery Tech. Bull. 25 (2004) 62–72.

[9] G. Cavallo, M. Aceto, R. Emmenegger, A.T. Keller, R. Lenz, L. Villa, S. Wörz, P. Cassitti, Preliminary non-invasive study of Carolingian pigments in the churches of St. John at Müstair and St. Benedict at Malles, Archaeol. Anthropol. Sci. 12 (2020), https://doi.org/10.1007/s12520-020-01024-2.

[10] I.N.M. Wainwright, E.A. Moffatt, P.J. Sirois, G.S. Young, Analysis of wall painting fragments from the Mogao and Bingling Grottoes, in: Conservation of Ancient Sites on the Silk Road, in: Proceedings of an International Conference on the Conservation of Grotto Sites, 1997, pp. 334–340.

[11] S. Aze, J.-M. Vallet, A. Baronnet, O. Grauby, The fading of red lead pigment in wall paintings: tracking the physico-chemical transformations by means of complementary micro-analysis techniques, Eur. J. Mineral. 18 (2006) 835–843, https://doi.org/10.1127/0935-1221/2006/0018-0835.

[12] C. Blänsdorf, S. Pfeffer, E. Melzl, The Polychromy of the Giant Buddha Statues in Bāmiyān, in: M. Petzet (Ed.), The Giant Buddhas of Bamiyan: Safeguarding the Remains Safeguarding the Remains, Berlin, 2009: pp. 237–264.

[13] S. Sotiropoulou, D. Bikiaris, C. Salpistis, G. Karagiannis, Y. Chryssoulakis, B.A. Price, J.H. Carlson, Panselinos' Byzantine wall paintings in the Protaton Church, Mount Athos, Greece: a technical examination, 2000.

[14] P.T. Moseley, I.M. Steele, The importance of the non-stoichiometry of lead dioxide and the location of hydrogen in the positive active mass of the lead–acid battery, J Energy Storage 61 (2023) 106754, https://doi.org/10.1016/j.est.2023.106754.

[15] X. Li, D. Pletcher, F.C. Walsh, Electrodeposited lead dioxide coatings, Chem. Soc. Rev. 40 (2011) 3879, https://doi.org/10.1039/c0cs00213e.

[16] I. Costantini, P.P. Lottici, D. Bersani, D. Pontiroli, A. Casoli, K. Castro, J. M. Madariaga, Darkening of lead- and iron-based pigments on late Gothic Italian wall paintings: Energy dispersive X-ray fluorescence, μ-Raman, and powder X-ray diffraction analyses for diagnosis: Presence of β-PbO2 (plattnerite) and α-PbO2 (scrutinyite), J. Raman Spectrosc. 51 (2020) 680–692, https://doi.org/10.1002/jrs.5817.

[17] E. Kotulanová, P. Bezdička, D. Hradil, J. Hradilová, S. Švarcová, T. Grygar, Degradation of lead-based pigments by salt solutions, J Cult Herit 10 (2009) 367–378, https://doi.org/10.1016/j.culher.2008.11.001.

[18] E. Avranovich Clerici, S. de Meyer, F. Vanmeert, S. Legrand, L. Monico, C. Miliani, K. Janssens, Multi-Scale X-ray Imaging of the Pigment Discoloration Processes Triggered by Chlorine Compounds in the Upper Basilica of Saint Francis of Assisi, Molecules 28 (2023), https://doi.org/10.3390/molecules28166106.

[19] D. Saunders, M. Spring, C. Higgitt, Colour change in red lead-containing paint films, in: 13th Triennial ICOM-CC Conference, Rio de Janeiro, 2002: pp. 455–463.

[20] Z.C. Kang, L. Machesky, H.A. Eick, L. Eyring, The solvolytic disproportionation of mixed-valence compounds: III. Pb3O4, J Solid State Chem 75 (1988) 73–89, https://doi.org/10.1016/0022-4596(88)90304-0.

[21] S. Daniilia, E. Minopoulou, A study of smalt and red lead discolouration in Antiphonitis wall paintings in Cyprus, Appl. Phys. A Mater. Sci. Process 96 (2009) 701–711, https://doi.org/10.1007/s00339-009-5163-9.

[22] M. Gutman, M. Lesar-Kikelj, A. Mladenovič, V. Čobal-Sedmak, A. Križnar, S. Kramar, Ramanmicrospectroscopic analysis of pigments of the Gothic wall painting from the Dominican Monastery in Ptuj (Slovenia), J. Raman Spectrosc. 45 (2014) 1103–1109, https://doi.org/10.1002/jrs.4628.

[23] C. Bolong, Y. Zongren, S. Manli, S. Zhongwei, Z. Jinli, S. Biwen, W. Zhuo, Y. Yaopeng, S. Bomin, Virtual reconstruction of the painting process and original colors of a color-changed Northern Wei Dynasty mural in Cave 254 of the Mogao Grottoes, Herit. Sci. 10 (2022), https://doi.org/10.1186/s40494-022-00785-4.

[24] S. Aze, J.-M. Vallet, O. Grauby, V. Detalle, P. Delaporte, Restauration des peintures au plomb par irradiation laser, TECHNIQUES DE L'INGÉNIEUR (2013) RE 224 1-11.

[25] T. de Seauve, V. Detalle, A. Semerok, S. Aze, O. Grauby, S. Bosonnet, K. Ginestar, J. M. Vallet, Continuous wave laser thermal restoration of oxidized lead-based pigments in mural paintings, Appl. Phys. B 127 (2021), https://doi.org/10.1007/s00340-021-07702-w.

[26] A.A. Mencaglia, I. Osticioli, S. Siano, Development of an efficient and thermally controlled Raman system for fast and safe molecular characterization of paint layers, Measurement (Lond) 118 (2018) 372–378, https://doi.org/10.1016/j.measurement.2017.11.056.

[27] I. Osticioli, A.A. Mencaglia, S. Siano, Temperature-controlled portable Raman spectroscopy of photothermally sensitive pigments, Sens. Actuators B Chem. 238 (2017) 772–778, https://doi.org/10.1016/j.snb.2016.07.104.

[28] F. Liggins, A. Vichi, W. Liu, A. Hogg, S. Kogou, J. Chen, H. Liang, Hyperspectral imaging solutions for the non-invasive detection and automated mapping of copper trihydroxychlorides in ancient bronze, Herit. Sci. 10 (2022) 142, https://doi.org/10.1186/s40494-022-00765-8.

[29] M. Cotte, V. Gonzalez, F. Vanmeert, L. Monico, C. Dejoie, M. Burghammer, L. Huder, W. de Nolf, S. Fisher, I. Fazlic, C. Chauffeton, G. Wallez, N. Jiménez, F. Albert-Tortosa, N. Salvadó, E. Possenti, C. Colombo, M. Ghirardello, D. Comelli, E.A. Clerici, R. Vivani, A. Romani, C. Costantino, K. Janssens, Y. Taniguchi, J. McCarthy, H. Reichert, J. Susini, The "Historical Materials BAG": A New Facilitated Access to Synchrotron X-ray Diffraction Analyses for Cultural Heritage Materials at the European Synchrotron Radiation Facility, Molecules 27 (2022), https://doi.org/10.3390/molecules27061997.

[30] Historical Materials BAG dataset repository, doi:10.15151/ESRF-DC-2115831341.

[31] J. Kieffer, V. Valls, N. Blanc, C. Hennig, New tools for calibrating diffraction setups, J. Synchrotron Radiat. 27 (2020) 558–566, https://doi.org/10.1107/S1600577520000776.

[32] V.A. Solé, E. Papillon, M. Cotte, Ph. Walter, J. Susini, A multiplatform code for the analysis of energy-dispersive X-ray fluorescence spectra, Spectrochim. Acta Part B At. Spectrosc. 62 (2007) 63–68, https://doi.org/10.1016/j.sab.2006.12.002.

[33] F. d'Acapito, G.O. Lepore, A. Puri, A. Laloni, F. La Manna, E. Dettona, A. De Luisa, A. Martin, The LISA beamline at ESRF, J. Synchrotron Radiat. 26 (2019) 551–558, https://doi.org/10.1107/S160057751801843X.

[34] L. Monico, F. d'Acapito, M. Cotte, K. Janssens, A. Romani, G. Ricci, C. Miliani, L. Cartechini, Total electron yield (TEY) detection mode Cr K-edge XANES spectroscopy as a direct method to probe the composition of the surface of darkened chrome yellow (PbCr1-xSxO4) and potassium chromate paints, Nucl. Inst. Methods Phys Res B 539 (2023) 141–147, https://doi.org/10.1016/j.nimb.2023.03.040.

[35] F. d'Acapito, A. Puri, G. Lepore, G. de Donatis, M.R. Cicconi, S.E. Ali, A. Fantin, D. Grandjean, S. Laureti, A. Marcelli, A. Martinelli, A. Menushenkov, Minguzzi. A., Activity report of the Italian CRG beamline at the European Synchrotron Radiation Facility (ESRF) - Year 2018, Zenodo (2022).

[36] B. Ravel, M. Newville, ATHENA, ARTEMIS, HEPHAESTUS: data analysis for X-ray absorption spectroscopy using IFEFFIT, J. Synchrotron. Radiat. 12 (2005) 537–541, https://doi.org/10.1107/S0909049505012719.

[37] D.L. Perry, T.J. Wilkinson, Synthesis of high-purity α- and β-PbO and possible applications to synthesis and processing of other lead oxide materials, Appl. Phys. A 89 (2007) 77–80, https://doi.org/10.1007/s00339-007-4073-y.

[38] E.M. Saurette, Y.Z. Frinfrock, B. Verbuyst, D.W. Blowes, J.M. McBeth, C.J. Ptacek, Improved precision in As speciation analysis with HERFD-XANES at the As K-edge: the case of As speciation in mine waste, J. Synchrotron Radiat. 29 (2022) 1198–1208, https://doi.org/10.1107/S1600577522007068.

[39] W.B. White, R. Roy, Phase Relations in the System Lead—Oxygen, J. Am. Ceram. Soc. 47 (1964) 242–249, https://doi.org/10.1111/j.1151-2916.1964.tb14404.x.

[40] J. Bouvaist, D. Weigel, Sesquioxyde de plomb, Pb2O3. I. Determination de la structure, Acta Crystallogr. Sect. A 26 (1970) 501–510, https://doi.org/10.1107/S0567739470001316.

[41] J.S. Anderson, M. Sterns, The intermediate oxides of lead, J. Inorg. Nucl. Chem. 11 (1959) 272–285.

[42] S. Kogou, G. Shahtahmassebi, A. Lucian, H. Liang, B. Shui, W. Zhang, B. Su, S. van Schaik, From remote sensing and machine learning to the history of the Silk Road: large scale material identification on wall paintings, Sci. Rep. 10 (2020), https://doi.org/10.1038/s41598-020-76457-9.

[43] K.L. Keester, W.B. White, Electronic spectra of the oxides of lead and of some ternary lead oxide compounds, Mat. Res. Bull. 4 (1969) 757–764.

[44] A. Suzuki, C.S. Cheung, Y. Li, A. Hogg, P.S. Atkinson, C. Riminesi, C. Miliani, H. Liang, Time and spatially resolved VIS-NIR hyperspectral imaging as a novel monitoring tool for laser-based spectroscopy to mitigate radiation damage on paintings, Analyst 149 (2024) 2338–2350, https://doi.org/10.1039/d3an02041j.

[45] D. Ciofini, J. Agresti, A.A. Mencaglia, S. Siano, I. Osticioli, Temperature sensing during Raman spectroscopy of lead white films in different purity grades and boundary conditions, Sens. Actuators B Chem. 325 (2020), https://doi.org/10.1016/j.snb.2020.128958.

[46] K.S.K. Varadwaj, M.K. Panigrahi, J. Ghose, Effect of capping and particle size on Raman laser-induced degradation of γ-Fe 2O 3 nanoparticles, J. Solid State Chem. 177 (2004) 4286–4292, https://doi.org/10.1016/j.jssc.2004.08.025.

[47] E. Mattei, G. De Vivo, A. De Santis, C. Gaetani, C. Pelosi, U. Santamaria, Raman spectroscopic analysis of azurite blackening, J. Raman Spectrosc. 39 (2008) 302–306, https://doi.org/10.1002/jrs.1845.

[48] I. Costantini, P.P. Lottici, K. Castro, J.M. Madariaga, Use of temperature controlled stage confocal raman microscopy to study phase transition of lead dioxide (Plattnerite), Minerals 10 (2020), https://doi.org/10.3390/min10050468.
[49] M. Vagnini, R. Vivani, E. Viscuso, M. Favazza, B.G. Brunetti, A. Sgamellotti, C. Miliani, Investigation on the process of lead white blackening by Raman spectroscopy, XRD and other methods: Study of Cimabue's paintings in Assisi, Vib. Spectrosc. 98 (2018) 41–49, https://doi.org/10.1016/j.vibspec.2018.07.006.
[50] L. Burgio, R.J.H. Clark, S. Firth, Raman spectroscopy as a means for the identification of plattnerite (PbO2), of lead pigments and of their degradation products, Analyst 126 (2001) 222–227, https://doi.org/10.1039/b008302j.
[51] S. Rahimi, O. Jahanbakhsh, I. Ahadzadeh, Effects of Pb2O3 nanoparticles on thermal and mechanical properties of epoxy resin, silicone, and PVC-based nanoshields, Prog. Nucl. Energy 169 (2024), https://doi.org/10.1016/j.pnucene.2024.105083.
[52] D.A. Ciomartan, R.J.H. Clark, L.J. McDonald, M. Odlyha, Studies on the thermal decomposition of basic lead(II) carbonate by Fourier-transform Raman spectroscopy, X-ray diffraction and thermal analysis, J. Chem. Soc. Dalton Trans. (1996) 3639–3645, https://doi.org/10.1039/DT9960003639.
[53] S. Pérez-Diez, A. Larrañaga, J.M. Madariaga, M. Maguregui, Unraveling the role of the thermal and laser impacts on the blackening of cinnabar in the mural paintings of Pompeii, Eur. Phys. J. Plus 137 (2022), https://doi.org/10.1140/epjp/s13360-022-03392-1.
[54] C. Genestar Juliá, C. Pons Bonafé, The use of natural earths in picture: study and differentiation by thermal analysis, Thermochim Acta 413 (2004) 185–192, https://doi.org/10.1016/j.tca.2003.10.016.